Microporous and Mesoporous Materials 378 (2024) 113249

Contents lists available at ScienceDirect

Microporous and Mesoporous Materials

journal homepage: www.elsevier.com/locate/micromeso

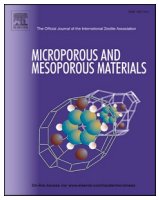

Gas self-diffusion in different local environments of mixed-matrix membranes as a function of UiO-66-NH_2 metal–organic framework loading

Omar Boloki [a], Stephen Dewitt [b], Eric T. Hahnert [b], Zachary Smith [b], Sergey Vasenkov [a,*]

[a] Department of Chemical Engineering, University of Florida, Gainesville, FL, 32611, USA
[b] Department of Chemical Engineering, Massachusetts Institute of Technology, Cambridge, MA, 02139, USA

ARTICLE INFO

Keywords:
Diffusion
PFG NMR
Mixed-matrix membranes
UiO-66-NH_2
Gas separations

ABSTRACT

This work focuses on quantification of microscopic self-diffusion of gas molecules in mixed-matrix membranes (MMMs) formed by dispersing UiO-66-NH_2 metal–organic framework (MOF) crystals in 6FDA-Durene polyimide. Self-diffusion measurements were performed by ^{13}C pulsed field gradient nuclear magnetic resonance (PFG NMR) for pure CO_2 and CH_4 with the spatial resolution in the range of 0.5–24 μm and for different MOF loadings between 12.5 and 50 weight percent. Diffusion measurements performed for each gas in the MMM with the lowest MOF loading of 12.5 weight percent yielded a single diffusivity for all measured diffusion times corresponding to a diffusion under the condition of a fast exchange between the UiO-66-NH_2 crystals and the surrounding polymer phase. However, as the UiO-66-NH_2 loading was increased, two molecular ensembles were observed for both CO_2 and CH_4: 1) an ensemble corresponding to diffusion inside UiO-66-NH_2 crystals and through the MOF–polymer interfaces, and 2) an ensemble corresponding to diffusion mainly in the polymer phase of the MMMs. This behavior can be explained by the formation of MOF clusters at higher MOF loadings. Quantification of the intra-cluster diffusivity, average cluster size, and the dependence of these properties on the MOF loading are presented and discussed. The reported measurements can serve as a framework to quantify discrete microscopic diffusion characteristics and sizes of interconnected MOF clusters in MMMs as MOF loading increases to reach the desired outcome of gas percolation over a spanning MOF cluster, viz a cluster of interconnected MOF crystals spanning an entire MMM.

1. Introduction

Membrane-based gas separations [1–4] represent a growing industrial technology that offers a potential alternative to conventional gas separation processes, including unit operations like amine-based absorption to capture CO_2 from various feed streams and cryogenic distillation for molecular fractionation [3,5]. Membrane technology can provide advantages such as improved energy efficiency, simple operation, potential cost savings, and a lower environmental impact in comparison to the current separation technologies [2,3,5]. However, all large-scale commercial gas separation membranes are made from polymers, and these materials are subject to an intrinsic tradeoff between permeability and selectivity [3,4] known as the Robeson upper bound [6,7]. One approach to overcome this intrinsic tradeoff is through the development of mixed-matrix membranes (MMMs), which can surpass polymer performance limits by incorporation of solid porous fillers [8–11]. MMMs combine separation performance advantages offered by the filler with the mechanical and scale-up properties of polymeric materials [3,5,9,12]. MMMs have been explored for applications in gas separations, heavy metal removal, water purification, and microfiltration, among others [13,14]. There are various types of fillers that can be used in MMMs, including zeolites, carbon molecular sieves (CMS), and metal–organic frameworks (MOFs). Recently, there has been a growing interest in research focusing on MMMs formed with MOF fillers. MOFs are composed of metals or metal–oxo clusters that are bridged by organic ligands [3,11,13]. MOFs exhibit great potential in gas separations due to their high chemical and thermal stability, as well as their ultra-high, uniform, and tunable porosity [3,14,15].

In recent years, the UiO-66 MOF [16,17], which contains zirconium–oxo clusters of $Zr_6O_4(OH)_4$ as metal nodes that are bridged by terephthalic acid (BDC) ligands, has attracted significant interest [15–17]. Beyond the native framework, the BDC ligands can be functionalized with a variety of derivatives, producing a range of functional UiO-66 MOFs, such as UiO-66-NH_2 and UiO-66-NO_2 [5,17–19]. Among

* Corresponding author.
E-mail address: svasenkov@che.ufl.edu (S. Vasenkov).

https://doi.org/10.1016/j.micromeso.2024.113249
Received 1 May 2024; Received in revised form 1 July 2024; Accepted 3 July 2024
Available online 4 July 2024

these structural analogs, the primary amine-functionalized MOF is of a particular interest. Cmarik et al. studied the adsorption properties of four different derivatives of UiO-66 [19] and revealed that UiO-66-NH_2 showed the highest uptake of CO_2, CH_4, and N_2 at 298 K. Thus, this MOF is of great interest for a variety of gas separation applications.

Quantifying transport properties of MMMs as a function of MOF loading is required to evaluate and optimize MMM separation performance. However, as composite materials, MMMs have different local environments, including regions of the polymer, filler, and corresponding interfaces. Typically, the effective macroscopic gas diffusion throughout the entire MMM is quantified through permeation, uptake, and related measurements [5,9,18]. Effective medium approaches (EMAs) are commonly used models to infer properties of each phase from the macroscopic measurements. Among these models, the Maxwell and Bruggeman models are most widely applied for MOF-based MMMs [20]. Unfortunately, these models infer permeabilities in the MOF phase based on macroscopic permeability measurements of the pure polymer and variable-loading MMMs. More direct approaches are needed to evaluate transport properties in each phase directly. Without such direct measurements, common model assumptions, such as the absence of polymer rigidification and the absence of polymer–MOF interfacial defect, cannot be verified, but only inferred [4]. Thus, to provide more direct and fundamental insights to transport in composite systems, especially insights related to interfacial phenomena, characterization of microscopic gas diffusion at relevant and localized length scales is needed. These data are exceedingly rare in the literature, leaving a key knowledge gap that is needed to support widely available macroscopic permeability, diffusion, and sorption data.

Pulsed field gradient nuclear magnetic resonance (PFG NMR) has been proven to be a technique of choice to quantify microscopic self-diffusion of light gases (i.e., CO_2, CH_4, C_2H_4, C_2H_6) in MMMs [10,12,21]. Previous PFG NMR studies of gas diffusion were performed with MMMs where fillers were crystals of zeolitic imidazolate frameworks (ZIFs), a subclass of MOFs. In this work, ^{13}C PFG NMR was applied to study microscopic self-diffusion of two industrial gases (CH_4 and CO_2) in MMMs containing UiO-66-NH_2 crystals with sizes of around 0.76 μm, which are somewhat larger than those typically used in MMMs. Using crystals with relatively large sizes of around 0.76 μm allowed us to quantify gas transport by PFG NMR on the length scales comparable with crystal sizes as well as on much larger length scales. In contrast to the previous PFG NMR studies of MMMs, the current work focuses on quantifying and understanding the dependence of intra-MMM microscopic diffusion as a function of increasing MOF loading in the MMM. The measurements were performed at high magnetic field of 17.6 or 14 T and at large magnetic field gradient amplitudes up to 23 T/m. The latter allowed performing PFG NMR measurements for displacements of gas molecules as small as 0.5 μm. All measurement results were then analyzed to determine different diffusion rates within the composite material for each gas over a range of molecular displacements and the corresponding diffusion times. For MMMs with sufficiently high MOF loadings these results allowed for the differentiation between diffusion within the MOF crystal aggregates and within the polymer region.

2. Experimental

2.1. Materials for mixed matrix membrane fabrication

Self-diffusion of CO_2 and CH_4 was studied in a dense film of 6FDA-Durene polyimide and the corresponding MMMs containing UiO-66-NH_2 MOF with the following MOF loadings i) 12.5 wt% ii) 25 wt% and iii) 50 wt%. 6FDA-Durene was purchased from Akron Polymer Systems and used without further purification. 6FDA-Durene was selected as the polymer for this study due to its high thermal stability, high glass-transition temperature, and a notable intrinsic CO_2/CH_4 separation performance [9]. 6FDA-Durene is also easily processible into not only flat sheet membranes but also into hollow fiber membranes, which are promising for industrial use [22]. UiO-66-NH_2 was synthesized by combining 410.0 mg of $ZrCl_4$ with 319.0 mg of 2-aminoterephthalic acid, 59.02 mL of glacial acetic acid (600 eq.), 100 μL of distilled water, and 140.9 mL of anhydrous dimethyl formamide (DMF). The reaction mixture was heated for 24 h at 393 K and then sonicated and centrifuged to collect the precipitated product. The product was subsequently washed twice with DMF, twice with methanol, and once with chloroform before suspension and storage in a chloroform solution.

2.2. Mixed matrix membrane fabrication

UiO-66-NH_2 nanoparticles suspended in chloroform were analyzed via TGA to determine the wt% of nanoparticles in suspension. An aliquot of this suspension was then separated and concentrated or diluted to reach a suspension of particles in 7.6 mL of chloroform. 6FDA-Durene was then added to the suspension such that the total weight of 6FDA-Durene and UiO-66-NH_2 totaled 380 mg, resulting in a casting solution of less than 5 wt%. This suspension was then left to mix on a roller table for 8 h before being cast with a filtered syringe into a glass Petri dish and covered by a glass plate. The suspension was then left to evaporate in a hood until a solid film was formed. This film was placed in a vacuum oven at 353 K for 12 h to remove any remaining solvent from the film. The fabrication of all MMMs followed the same effective casting procedure, regardless of the MOF loading. It is important to note, however, that fabricating MMMs with the MOF loading of 50 wt% resulted in more brittle membranes, but the material still formed unbroken circular films with approximately 5 cm in diameter.

2.3. Characterization

The structure of the UiO-66-NH_2 nanoparticles was analyzed using a FEI Tecnai multipurpose transmission electron microscope (TEM). The nanoparticles were observed by diluting two drops of a suspension of UiO-66-NH_2 in 10 mL methanol and applying the suspension to a PELCO 100 mesh copper grid acquired from Ted Pella. Images obtained from these micrographs were then analyzed using Image J software to determine particle size distributions (Fig. S1). The crystallinity of the MOF particles in powder form was analyzed using a Rigaku Smartlab multipurpose x-ray diffractometer (XRD) in the 2θ region from 5 to 50°. The cross-sectional morphologies of all MMM films were observed using a Zeiss Merlin high-resolution scanning electron microscope (SEM) after the films were fractured under liquid nitrogen.

2.4. Preparation of NMR samples

To prepare PFG NMR samples, films were cut into strips of 2–3 mm in width and 5–10 mm in height. To prepare each sample, around 100 mg of strips were packed in a 5 mm medium walled NMR tube (Wilmad Labglass, Inc). The NMR tube was then connected to a custom-made vacuum system, where the sample was degassed at 373 K for 8 h under high vacuum to ensure that the films were sorbate free before testing. After activation, the sample remained under vacuum and was cooled to ambient temperature (298 K). Single component gases (CH_4 or CO_2) were loaded into the sample through cryogenic condensation with the desired amount of gas using liquid nitrogen. Following sorbate loading, the NMR tube was flame sealed and disconnected from the vacuum system. To ensure sorption equilibrium at an ambient temperature of 298 K, NMR tubes were left at this temperature for at least 8 h after loading before performing any experiments. The sorbates selected for the study were ^{13}C enriched CO_2 and CH_4. Both sorbates were of 99 % isotopic purity (Sigma Aldrich).

Before any NMR measurements, each sample was kept for at least 1 h in the NMR spectrometer at the desired measurement temperature (either 253 or 308 K) to ensure sorption equilibrium. To confirm the time selected (1 h) was sufficient to reach the sorption equilibrium selected experiments were repeated after several hours to check the

reproducibility of the results. It was confirmed that the results remained unchanged, within uncertainty, including no change in the sorbate intra-membrane concentrations, which were determined as discussed below.

Sorbate loadings were estimated using NMR spectroscopy (Tables S1–S6) taking advantage of the proportionality of the area under the NMR spectrum and the number of the corresponding sorbate molecules in the sample, as is in our previous studies [10,21,23,24]. NMR measurements of reference samples containing only bulk gases at a known pressure with no MMM added were performed to obtain the proportionality constants between the amount of sorbate and the area under the NMR spectrum. The total NMR signal measured in the MMM samples contained contributions from molecules located in the intra-membrane region and the surrounding bulk gas phase of the sample. These relative contributions were quantified using a mass balance with the following known properties: (i) volume of the sealed NMR tube, (ii) total mass of the gas in the NMR tube, (iii) the total volume and mass of the film samples, and the volume of the surrounding gas phase in the active range of the NMR radiofrequency coil. The intra-membrane gas concentrations calculated using this approach are presented in Tables S3–S6. These concentrations can also be quantified based on the ^{13}C T_2 NMR measurements [25,26] if the intra-membrane and bulk gas phase fractions exhibit different T_2 values, as was the case for the samples loaded with CH_4. For this gas, the ^{13}C T_2 NMR measurements yielded two molecular ensembles with different T_2 NMR relaxation times and the corresponding fractions (Table S7). These molecular ensembles were attributed to the molecules inside the film and the molecules in the bulk gas phase between the film pieces (cf., Table S7). Multiplying the fraction related to the intra-membrane component with the total mass of the gas obtained by NMR for the sample region containing the MMM provided an estimation of the intra-membrane concentration. This approach yielded the same intra-membrane concentration for methane, within uncertainty, as that based on the mass balance (Tables S4 and S6). The method based on the ^{13}C T_2 NMR measurements could not be used for CO_2 because for this gas only a single T_2 NMR relaxation time was measured in the studied MMM samples.

2.5. PFG NMR measurements

NMR measurements were performed mainly using a 14 T Avance III spectrometer (Bruker Biospin) and selected measurements were performed using a 17.6 T Avance III HD spectrometer (Bruker Biospin) operating at ^{13}C frequencies of 149.8 MHz and 188.6 MHz, respectively. The magnetic field gradients with amplitudes up to 23 T/m were generated using a *Diff30* diffusion probe at 14 T and a *Diff50* diffusion probe at 17.6 T. Selected experiments were also performed using a *DiffBB* diffusion probe at 14 T to ensure the reliability and consistency of the data. The relatively high maximum magnetic field gradient strength allowed diffusion to be quantified for molecular displacement as small as 0.5 μm, which was recorded for gas molecules diffusing mostly in the polymer phase of the MMMs. No significant differences were observed between the data measured using the two spectrometers and the different diffusion probes, confirming the absence of any measurement artefacts. Bipolar, sine and trapezoidal shaped magnetic field gradient pulses were used with effective pulse durations between 1.4 ms and 3 ms. In most cases, sinusoidal shaped gradient pulses were used. To achieve a larger area under a gradient pulse for a fixed pulse duration ≥1.8 ms sinusoidal pulses were frequently replaced by trapezoidal pulses. This was done for PFG NMR measurements of samples with lower diffusivities to achieve sufficiently large signal attenuations. It is important to note that the gradient pulse shape and duration remained unchanged in the measurements of any particular PFG NMR attenuation curve. The total time needed to perform a PFG NMR measurement to obtain a single self-diffusivity value ranged between 1 and 6 h with a total number of scans between 144 and 512, depending on the signal to noise ratio. The repetition delays used were between 3 and 6 s, which is at least 1.5 times greater than the T_1 relaxation time. The diffusion time ranged from 7 ms to 1.28 s for both CO_2 and CH_4 diffusion. ^{13}C PFG NMR was used rather than the more common ^{1}H PFG NMR to take advantage of the longer T_2 relaxation time of the ^{13}C nuclei of guest molecules in MMMs. The ^{13}C NMR spectrum for CO_2 and CH_4 consisted of a single non-overlapping line with chemical shifts of around 150 and 4 ppm, respectively.

The diffusion experiments were conducted using the 13-interval pulse sequence [27] using bipolar gradients that were modified with the addition of a longitudinal eddy current delay [28]. This sequence was used to minimize or eliminate inhomogeneities in the magnetic field (*i.e.,* magnetic susceptibility effects). Such inhomogeneities are expected for heterogeneous systems such as stacked film pieces that were used in this work. Each self-diffusivity was obtained from the dependence of the normalized PFG NMR signal on the amplitude of the magnetic field gradient (g). This dependence is known as a PFG NMR attenuation curve, which, in the case of normal diffusion when all studied molecules diffuse with the same self-diffusion coefficient, can be described by the following equation [29]:

$$\psi = \frac{S(g)}{S(g \sim 0)} = \exp\left(-q^2 D t\right), \tag{1}$$

where ψ is the PFG NMR signal attenuation, S is the PFG NMR signal at gradient strength g, t is the diffusion time (*i.e.,* the diffusion observation time) [27] and $q = 2\gamma\delta g$, where γ, is the gyromagnetic ratio, and δ is the effective duration of one gradient pulse. In the case of three-dimensional diffusion, the root mean square displacement (RMSD) can be related to the self-diffusivity by using the Einstein relation [29]:

$$< r^2 >^{1/2} = \sqrt{6Dt}, \tag{2}$$

In the case of two molecular ensembles diffusing with different self-diffusivities the attenuation equation can be written as follows:

$$\psi = \frac{S(g)}{S(g \sim 0)} = \sum_{i}^{n=2} p_i \exp\left(-D_i q^2 t\right), \tag{3}$$

where p_i and D_i are, respectively, the population fraction and the self-diffusivity of ensemble i. The self-diffusivities and the fractions were calculated by fitting and using least-squares regression to Eq. (3) on the measured PFG NMR attenuation curves with the constraint that $\sum p_i = 1$. The experimental error was determined by considering the following: (i) the reproducibility of data when measurements of the same sample were performed using the different spectrometers (14 T and 17.6 T) under the same experimental conditions and (ii) the reproducibility of data from measurements under the same experimental conditions of two identically prepared (but different) samples. The total experimental uncertainty was around 25 % under most experimental conditions.

Longitudinal (T_1) and transverse (T_2) ^{13}C NMR relaxation times of the sorbates were determined using the standard inversion recovery and standard Carr-Purcell-Meiboom-Gill (CPMG) pulse sequences, respectively. The tau value used in the CPMG experiments was 100 μs. T_1 measurements showed the presence of 2 ensembles with different T_1 times; one ensemble was attributed to molecules mostly diffusing inside the membrane film and the second to the molecules mostly diffusing in the gas phase outside the membrane film (Table S7). It is important to note that due to relatively large T_1 measurement times there is a significant exchange between the film and gas phase environments. The ensemble assignment was based on the comparison with the corresponding relaxation data obtained for the pure bulk gas phase (no membrane film added). The two ensembles were observed for both methane and carbon dioxide under our T_1 measurement conditions. Table S7 shows the T_1 results obtained for different samples studied. In the case of T_2 NMR relaxation measurements, two molecular ensembles with different T_2 times were observed only for methane. These ensembles were attributed to gas molecules located inside and outside the film.

Biexponential fitting was used to quantify the fractions and their corresponding T_2 relaxation times for the MMM samples. The ensembles were assigned in the same way as identified above for T_1. The relaxation measurements were also conducted for pure 6FDA-Durene films loaded with single-component gases (Table S8). All NMR relaxation data are presented in Tables S7 and S8.

3. Results and discussion

Fig. 1 shows pXRD patterns of UiO-66-NH_2 crystals. The data in the figure demonstrate good crystallinity of the MOF and a good agreement with the corresponding simulated pattern. Fig. 2 shows SEM cross-sectional images of the 6FDA-Durene film and the MMMs with different UiO-66-NH_2 loadings used. The images of the MMMs with the two largest MOF loadings of 25 wt% and 50 wt% show some evidence of defects at the MOF-polymer interfaces. In particular, void cages can be seen around MOF crystals in Fig. 2C. Fig. 2D shows evidence of MOF crystal aggregates with some voids between MOF crystals. Interfacial defects will be discussed more later in the paper in connection with the reported PFG NMR results. Diffusion measurements were first performed for the MMM with 12.5 wt% loading of UiO-66-NH_2, which corresponds to approximately 14 vol%. In this membrane significant space between neighboring MOF crystals is expected, on average. Thus, these experiments are useful in evaluating if MOF crystals are evenly dispersed, which will result in monoexponential PFG NMR attenuation curves under the conditions of fast exchange between MOF crystals and the polymer phase.

Fig. 3 shows examples of the ^{13}C PFG NMR attenuation curves measured for CO_2 and CH_4 diffusing in a 12.5 wt% UiO-66-NH_2/6FDA-Durene MMM for diffusion times in the range between 7 and 640 ms at 308 K. Additional examples of ^{13}C PFG NMR attenuation curves for measurements performed with these samples at a lower temperature of 253 K are presented in the Supplementary Materials section (Fig. S2). While these experiments and most of the experiments to be presented later were conducted at 14 T, some additional experiments were performed at a higher magnetic field of 17.6 T to confirm that no measurement artefacts were present. The observed coincidence of the data, within uncertainty, confirms the reproducibility and reliability of the measured results (see examples in Fig. 3). It can be seen in Fig. 3 and S2 that the attenuation curves for both CO_2 and CH_4 exhibit a mono-exponential behavior (i.e., linear in the semi-logarithmic representation of the figures) and no dependence on diffusion time. This observed behavior agrees well with Eq. (1), as can be observed by the average fitted lines to this equation in the figures.

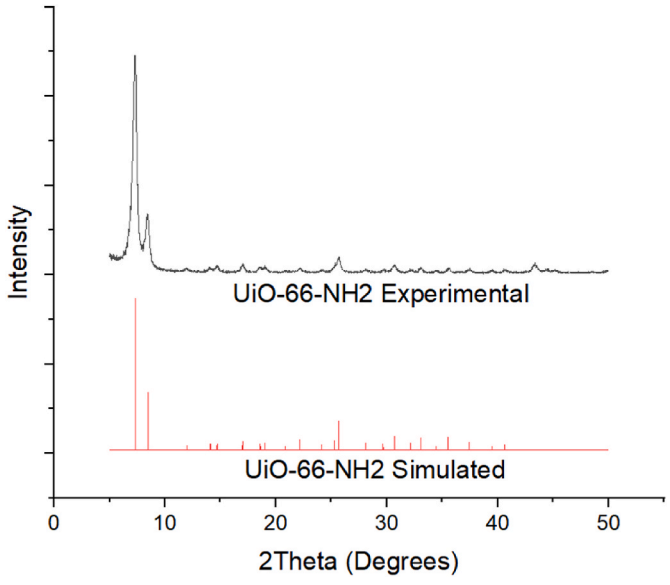

Fig. 1. pXRD pattern of UiO-66-NH_2 crystals performed over a range of 5-50° 2θ.

These lines correspond to single self-diffusivities independent of the diffusion time for each sorbate, sample, and temperature. Based on these data it can be concluded that the membrane transport properties remain uniform within the studied range of diffusion times (7–640 ms) and within the corresponding values of RMSDs (0.5–13 μm), which indicate uniform distribution of UiO-66-NH_2 crystals and no substantial interfacial defects. The values of gas self-diffusivities and the corresponding RMSD ranges are shown in Table S9. The RMSD values were comparable with or larger than the average crystal size (0.76 μm) thus confirming the conditions of fast exchange between the UiO-66-NH_2 crystals and the polymer phase under our PFG NMR measurement conditions.

The diffusion data for 12.5 wt% UiO-66-NH_2/6FDA-Durene MMM (Table S9) were compared with the corresponding gas self-diffusivities in a pure 6FDA-Durene polymer film at similar sorbate loading pressures (Fig. S3 and Table S10). The gas self-diffusivities in the MMM at 308 K (5×10^{-11} m^2 s^{-1} for CO_2, and 2.2×10^{-11} m^2 s^{-1} for CH_4) were observed to be higher than the corresponding self-diffusivities in the pure polymer (2.8×10^{-11} m^2 s^{-1} for CO_2, and 1.1×10^{-11} m^2 s^{-1} for CH_4). Higher self-diffusivities in the MMM can be due to changes of the properties of the polymer phase in the MMM in comparison to the pure polymer film, presence of some interfacial MOF-polymer defects (Fig. 2), as well as the conditions of fast exchange between the polymer and MOF phases [10,25]. As a result of such fast exchange, gas self-diffusivities in MMMs have some contributions from the intra-MOF self-diffusivities [21,29], which are larger than those in the polymer phase.

In terms of transport performance, the largest benefits for MMMs occur at high MOF loadings [3]. However, it is exceedingly difficult to capture *in situ* data on diffusion within discrete phases of these composites [25,30]. Given this limitation, most reports in the literature infer the transport properties of MOF materials within an MMM by applying models, the most common of which is the Maxwell model. Unfortunately, validating and improving these models is impossible without directly accessing data on the underlying transport properties in different local environments within these composite materials. Our aim in this study is to extract quantifiable diffusion information within the polymer- and MOF-rich domains of these MMMs, which provides direct *in situ* data on transport properties within each phase. To accomplish this goal, we investigated higher MOF loadings, which should result in larger quantities of MOF-rich domains, potentially enabling a deconvolution of diffusion properties within the PFG NMR attenuation curves. In terms of MOF loading, our 25 wt% and 50 wt% samples correspond to loadings of 28 vol% and 54 vol%, respectively, so we are within the loadings where clustering of the MOF crystals can become significant. Previous studies by Vasenkov et al. have used ^{13}C PFG NMR to determine *in situ* transport properties for ZIF crystals inside MMMs [10,21,26]. Polymer penetration into MOF materials has also been probed using similar techniques, including work by Duan et al. [31], who used ^{13}C NMR to probe the penetration of poly(ethylene oxide) oligomers into UiO-66. However, to the best of our knowledge, no work has previously been done to capture *in situ* data on the transport properties of UiO-66-NH_2 based MMMs.

Fig. 4 shows the ^{13}C PFG NMR attenuation curves for CO_2 and CH_4 diffusing in the MMMs with the higher MOF loadings of 25 wt% and 50 wt% for diffusion times in the range of 7–1280 ms at 308 K. As seen in Fig. 4, the coincidence of the data measured at 14 T and 17.6 T indicates that our experiments are free of any magnetic susceptibility effects or any other measurement artefacts. In contrast to the data obtained for the lower MOF loading (Fig. 3), the PFG NMR attenuation curves in Fig. 4 show clear deviations from the mono-exponential behavior. These deviations are more pronounced at short diffusion times and become much smaller at higher diffusion times. In the limit of large diffusion times, mono-exponential behavior (*i.e.*, linear in the presentation of Fig. 4) was observed. Such behavior indicates the presence of at least two molecular ensembles diffusing with two different self-diffusivities at small

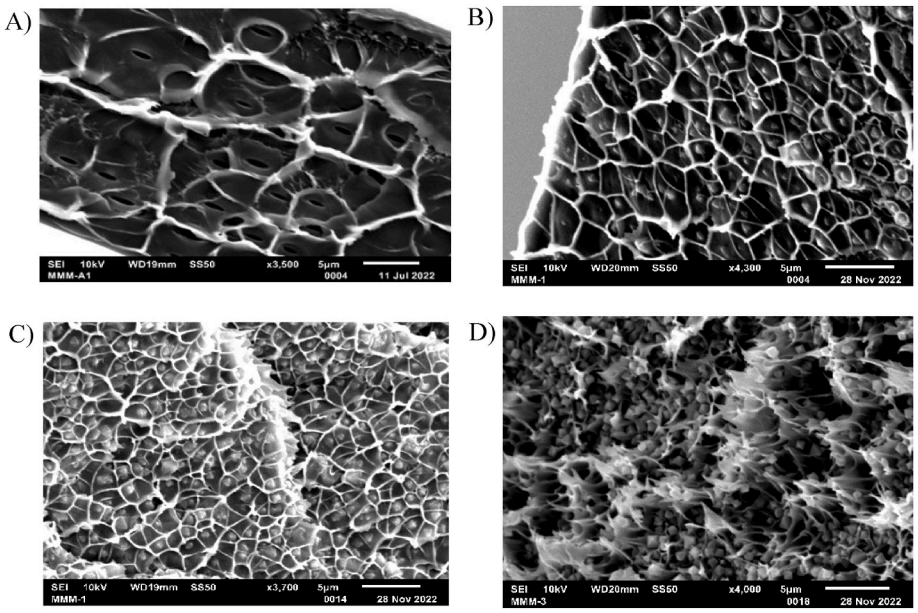

Fig. 2. SEM cross-sectional images of 6FDA-Durene membranes containing (A) 0 wt% (B) 12.5 wt% (C) 25 wt% (D) 50 wt% of well dispersed UiO-66-NH_2 crystals averaging 764 nm in size.

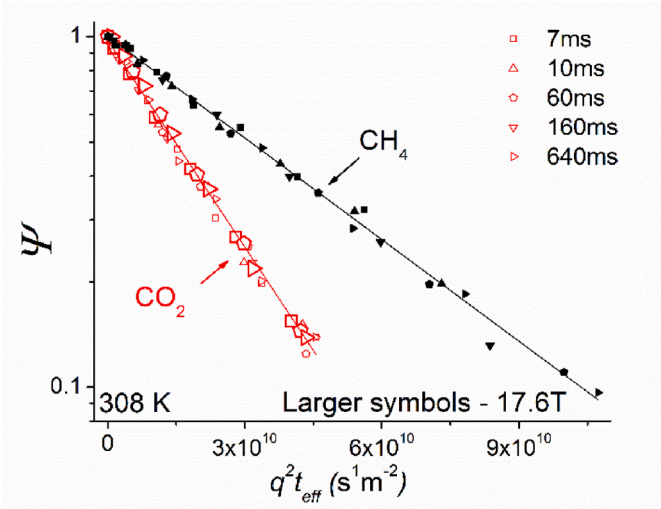

Fig. 3. ^{13}C PFG NMR attenuation curves measured in a 12.5 wt% UiO-66-NH_2/6FDA-Durene MMM loaded with CO_2 (empty symbols) and CH_4 (filled symbols) at 308 K. All measurements were performed at 14 T unless indicated otherwise in the figure.

diffusion times, while fast molecular exchange between different membrane environments is approached in the limit of large times. Analogous to our previous studies of MMMs [10,21,25] we used Eq. (3), which assumes the existence of two molecular ensembles with different diffusivities, to fit the non-mono-exponential attenuation curves in Fig. 4. The results of least square fitting using Eq. (3) can be seen in Supplementary Materials section (Table S11).

Under our measurement conditions, the PFG NMR signal from the gas molecules diffusing outside the membrane films is attenuated at the smallest gradient strength used, eliminating any bulk gas-phase influence on the measured signal. Therefore, the deviations from the mono-exponential behavior can be explained only by the existence of different molecular ensembles inside the MMMs. The two intra-membrane ensembles observed in the measurements were attributed to molecules diffusing mostly inside MOFs and through MOF–polymer interfaces (ensemble 1 with a faster diffusivity, D_1), and to molecules mostly diffusing inside the polymer phase (ensemble 2 with a slower diffusivity, D_2). This assignment was confirmed by the observation that the diffusivities of intra-polymer ensemble 2 were approaching the corresponding diffusivities measured in a pure 6FDA-Durene polymer (compare data presented in Tables S10 and S11). The PFG NMR observation of ensemble 1 under the conditions when RMSDs significantly exceed the size of a single MOF crystal provides evidence for the formation of MOF clusters, which can be expected at higher MOF loadings that were used (Fig. 2). The self-diffusion data measured at a lower temperature of 253 K similarly showed the trend of a transition from a bi-exponential behavior to that approaching mono-exponential at longer diffusion times, thus confirming our conclusion about the existence of the two ensembles of gas molecules related to MOF clustering in the MMMs (Fig. S4).

The measured self-diffusivities D_1 of ensemble 1 are expected to approach at short diffusion times the corresponding self-diffusivities inside single MOF crystals, viz. intracrystalline self-diffusivities. Due to a relatively small size of UiO-66-NH_2 crystals used in the current study, intracrystalline self-diffusivities of CO_2 and CH_4 could not be measured directly by PFG NMR. To our knowledge, such diffusivities were also not reported in the literature. However, intracrystalline self-diffusivities of CO_2 and CH_4 were measured by QENS in UiO-66 [32]. These self-diffusivities were observed to be slightly larger than the reported D_1 values at comparable temperatures. The difference can be related to the presence of –NH_2 groups in UiO-66-NH_2. These groups enhance interactions with CO_2 and can reduce the effective pore size. Interactions of CO_2 molecules with the –NH_2 groups in UiO-66-NH_2 are relatively weak and correspond to physisorption [19]. No evidence of chemisorption and/or reaction between these groups and CO_2 molecules was observed. As a result, all CO_2 molecules diffusing in MOF crystals are expected to visit multiple –NH_2 groups on the millisecond time scale of the PFG NMR measurements. Clearly, CO_2 interactions with –NH_2 groups are expected to reduce values of the CO_2 self-diffusivities and RMSDs measured for particular diffusion times.

The dependencies of the measured self-diffusivities on the diffusion time of CO_2 and CH_4 in the different MOF loading MMMs at 308 K are presented in Fig. 5. The corresponding plots for 253 K can be seen in Fig. S5. Fig. 5A shows a single self-diffusivity for each gas plotted as a function of diffusion time for a 12.5 wt% UiO-66-NH_2/6FDA-Durene

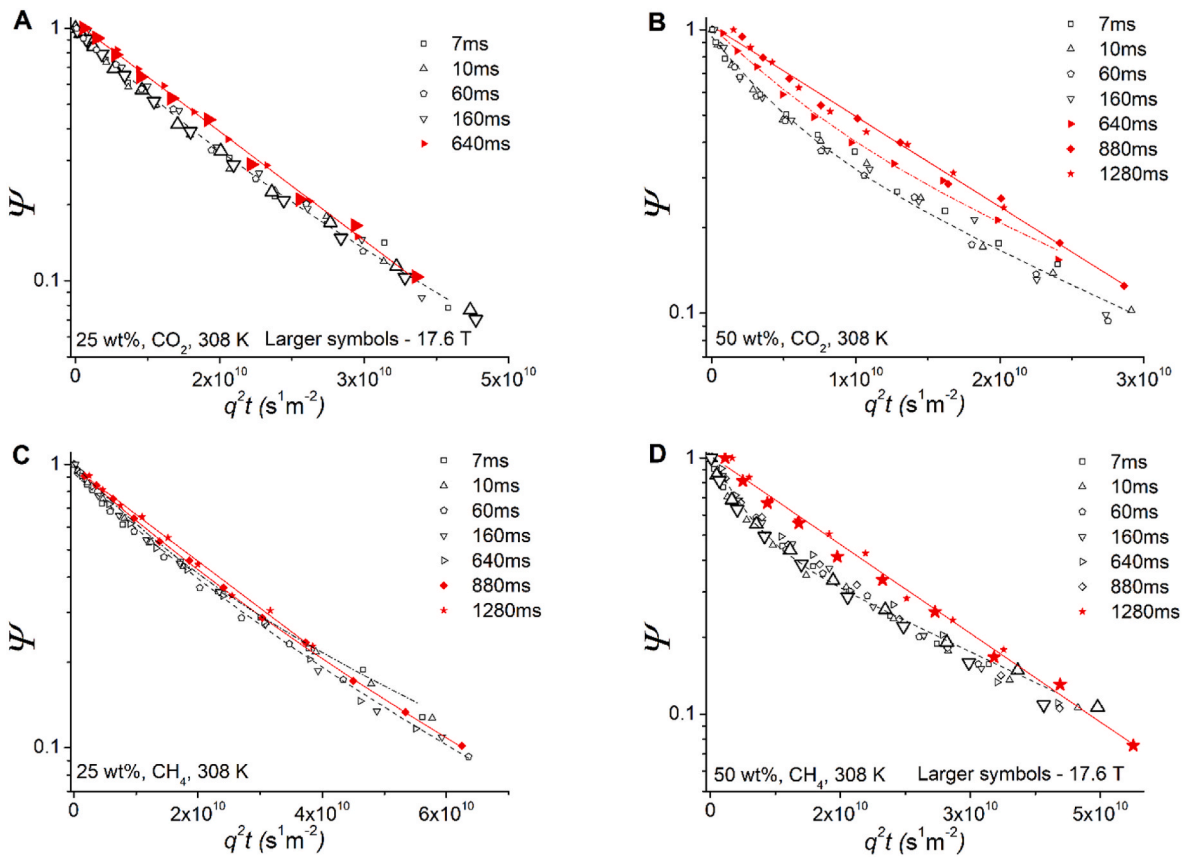

Fig. 4. ^{13}C PFG NMR attenuation curves measured in 25 wt% (A, C) and 50 wt% (B, D) UiO-66-NH_2/6FDA-Durene MMMs loaded with CO_2 (A, B) and CH_4 (C, D) performed at 14 T (unless indicated otherwise in the figure) using the 13-interval PFG NMR pulse sequence at 308 K. Solid symbols were used for attenuation curves consistent with the mono-exponential decay, within uncertainty. Solid lines represent the results of least-square fitting using Eq. (1). Dashed lines represent the results of least-square fitting using Eq. (3).

MMM. In this case there is no or little MOF crystal clustering, and the condition of fast exchange between the MOF and polymer phase is fulfilled for each measured diffusion time. Clearly, in this case there is also no dependence on RMSD (Figs. S6A and S7A). This result also provides evidence of uniform transport properties of the membrane for the range of the RMSD values used. Fig. 5B and C shows the dependencies of the self-diffusivities of the ensembles 1 and 2 discussed above on diffusion time.

In the limit of large diffusion times the diffusivities of both ensembles approach the same value corresponding to a fast exchange between different membrane environments. The data in these figures can be used to estimate the sizes of MOF clusters in the MMMs with 25 wt% and 50 wt% MOF loadings. This size is expected to be approximately equal to the RMSD at the point of convergence where two diffusivities merge into a single value. In the case of the MMM loaded with 25 wt% MOF, the estimated cluster size for CO_2 was approximately 16 ± 2 μm, and around 17 ± 2 μm for CH_4. These values are the same, within uncertainty. This observation supports the interpretation of our data because the MOF cluster size should not depend on the sorbate type. For the 50 wt% MMM, larger cluster sizes were estimated, approximately 20 ± 2 μm for CO_2 and around 21 ± 2 μm for CH_4. Some increase in the cluster size for the 50 wt% MMM is expected due to a higher concentration of UiO-66-NH_2 crystals in this sample. It is important to note that the cluster sizes were estimated based only on the data for 308 K. The maximum measured RMSDs were somewhat smaller at a lower temperature of 253 K, which precluded the evaluation at conditions where D_1 and D_2 are the same.

Under our experimental conditions, the CO_2 self-diffusivity in all three studied MMMs shows a tendency to be higher than the corresponding self-diffusivity of CH_4 when compared for the same molecular ensemble, MMM sample, and temperature. This tendency is more pronounced for the intra-polymer ensemble (ensemble 2) than for the intra-MOF ensemble (ensemble 1). The observed diffusivity difference can be understood based on the smaller size of CO_2 (3.3 Å) molecules in comparison to CH_4 molecules (3.8 Å) [33].

Fig. 6 shows self-diffusivities plotted as a function of the MOF loadings in the MMMs for two temperatures (308 and 253 K) at a diffusion time of 10 ms, which represents the smallest diffusion time limit common for all studied samples. This diffusion time was selected to minimize the influence of molecular exchange between different MMM environments on the measured diffusivities. It is seen that the faster self-diffusivity (D_1) increases with increasing MOF loading.

This finding can be attributed to a larger extent of MOF crystal clustering and/or formation of some free volume defects at the interfaces between MOF crystals as the MOF loading increases (Fig. 2). At the same time, the slower diffusivity (D_2) which is related to molecules diffusing mostly in the polymer phase remains the same, within uncertainty. The latter diffusivity is similar to that in the pure polymer film without MOF (Fig. S8). In gas separations, diffusion selectivity can be defined as the ratio of intra-membrane diffusivities for the studied pair of sorbates. This information can be gleaned from Fig. 6, which shows that the average diffusion selectivity for ensemble 1 (intra-MOF diffusion) is only around 2. As the MOF loading increases, the diffusion selectivity for this ensemble stays roughly the same or even decreases. This result is not surprising when considering the sizes of CO_2 and CH_4 (3.3 and 3.8 Å, respectively), which are significantly smaller than the UiO-66-NH_2 pore aperture size (around 6 Å) [34], so no large size-sieving effects and fast gas diffusion are expected. The small

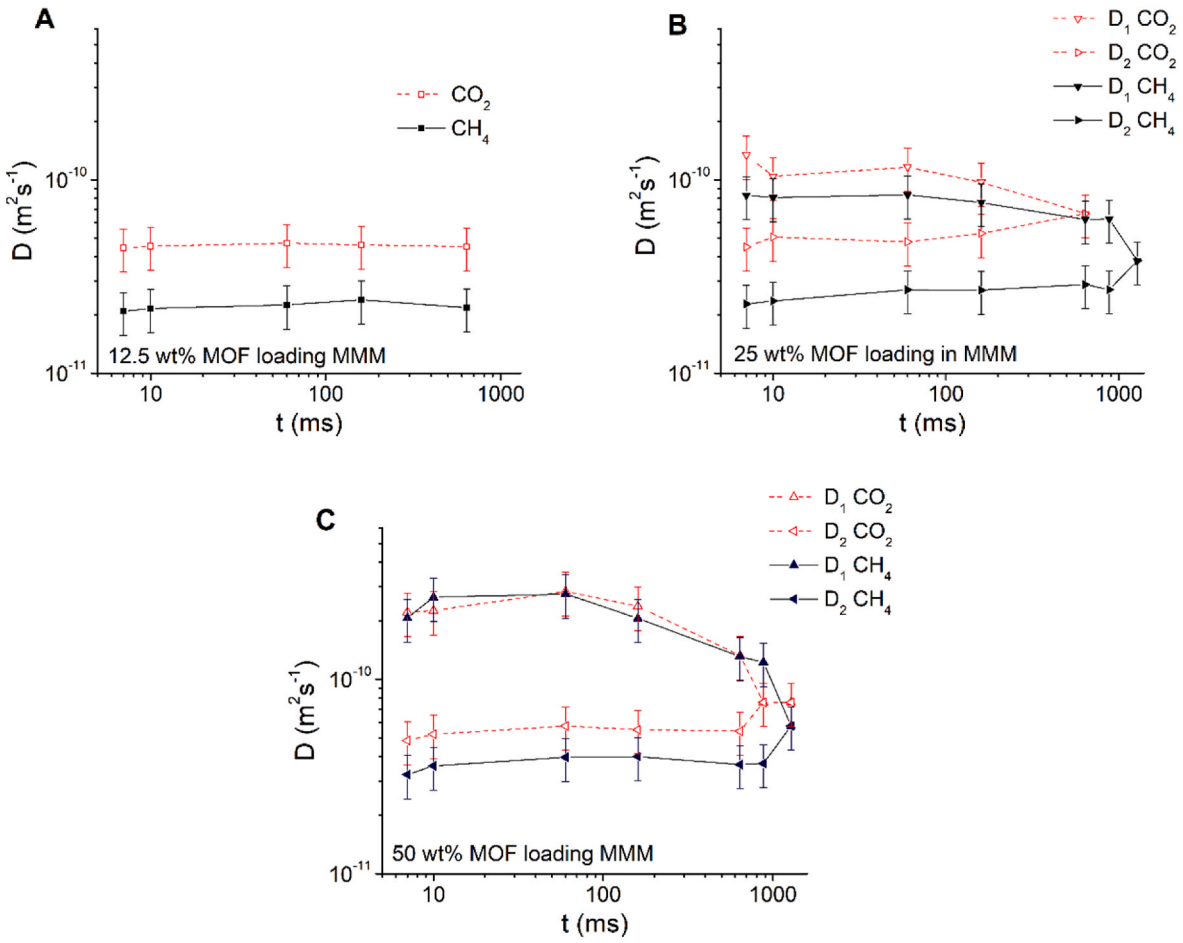

Fig. 5. CO_2 (empty symbols) and CH_4 (filled symbols) self-diffusivities plotted as a function of diffusion time in UiO-66-NH_2/6FDA-Durene MMM samples with MOF loadings of 12.5 wt% (A), 25 wt% (B), and 50 wt% (C) at 308 K. D_1 and D_2 represent the self-diffusivities of ensembles 1 and 2, respectively, discussed in the text.

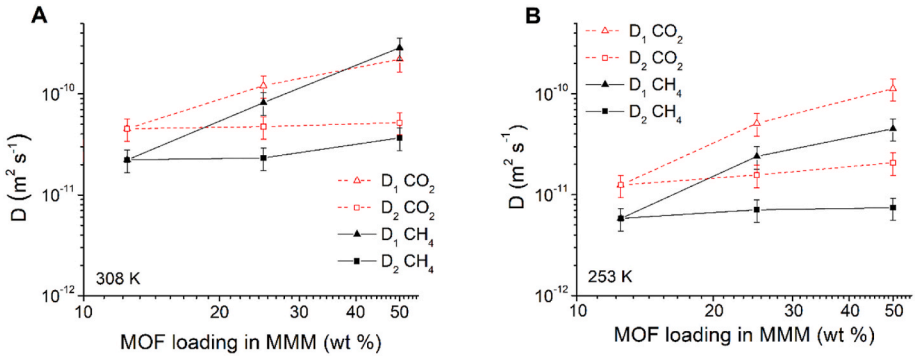

Fig. 6. Self-diffusivities of CO_2 (empty symbols) and CH_4 (filled symbols) in the limit of small diffusion time (10 ms) plotted as a function of MOF loading in the MMM for 308 K (A) and 253 K (B).

diffusion selectivity observed for ensemble 1 (intra-MOF diffusion) is also consistent with an occurrence of some free volume defects at the interfaces between neighboring MOF crystals (Fig. 2). The gas diffusivity values and diffusion selectivity for ensemble 2 (intra-polymer diffusion) remains constant, irrespective of an increase in the MOF loading (Fig. 6). The latter result indicates that the polymer properties governing diffusion of the studied gases in the polymer phase remain mostly unchanged as the MOF loading increases. It is important to note that the MMM type selected for this work is promising for CH_4/CO_2 separations mostly due to a remarkable sorption selectivity [9,18], which is not studied in this work.

To ensure the validity of the presented comparison between the CH_4 and CO_2 self-diffusivities, which were measured at slightly different intra-MOF and intra-MMM loadings, complementary PFG NMR measurements were conducted at several different gas intra-membrane concentrations. These studies confirmed that minor deviations in the gas concentrations do not significantly affect the results of the analysis of the diffusivities across different samples. The data presented in Figs. S8 and S9 reveal a lack of any significant gas concentration dependence of the measured self-diffusivities.

The activation energy of diffusion was estimated by analyzing the self-diffusivity data at two different temperatures. While the

experimental uncertainty is relatively large, Table S12 shows that there is no significant dependence of the activation energy of diffusion on the MOF loading for any particular gas type and molecular ensemble (intra-MOF or intra-polymer). However, the activation energy data show a tendency of a higher activation energy for CH_4 than for CO_2 for the intra-MOF ensemble. This observation can be attributed to a larger molecular size of the former gas.

The performance of MOF-based MMMs depends significantly on MOF composition and MOF loading, but there are few studies that quantify MOF clustering effects, and – to the best of our knowledge – none that reported direct measurements of diffusion inside MOF clusters for UiO subclass of MOFs or any other MOF type. In this study, our findings reveal the formation of two phases: a MOF-rich phase with effective domain sizes large enough to be observed within the resolution of PFG NMR and a polymer phase. Interestingly, the features for the MOF-rich phase become apparent for MOF loadings $\geq$25 wt% ($\geq$28 vol %), and the theoretical percolation threshold (0.31 for site percolation of randomly packed hard spheres) is expected to occur in the same range of MOF loadings, assuming the MOF particles are approximated as spheres [35]. For the highest (50 wt%) MOF loading MMM our PFG NMR data discussed above show percolation over the MOF phase with no significant transport resistance from interfaces between neighboring MOF crystals up to a length scale of around 20 μm, which is more than 26 times larger than the average size of MOF crystals. This result is consistent with the SEM image in Fig. 2d, which shows some crystal clustering and poor interfacial morphology between some crystals in this very high-loading MMM. However, for the displacement length scales larger than around 20 μm the transport resistance from the polymer phase between MOF crystals becomes more significant, resulting in a decrease in gas self-diffusivities. Hence, no indication of an interconnected MOF cluster spanning an entire MMM was observed for either CO_2 or CH_4. This finding suggests a mechanism of physical priming for some MOF crystals during the preparation of casting solutions followed by cluster formation. Physical priming is the phenomenon of polymer adsorption onto MOFs to form a soft polymer shell when suspensions are prepared [36]. Thus, for MOF crystals affected by physical priming there is some mass transfer resistance from the polymer at the MOF interface that precludes significant MOF–MOF contact. The existence of such resistance is common in other MMMs formed with 6FDA-based polyimides. Notably, Zhang et al. studied MMMs formed from ZIF-8 and 6FDA-DAM with loadings up to 48 wt% for propylene/propane separations and observed continuous increases in permeability and selectivity without a step change in permeability that would be characteristic of diffusion effects at percolation [37].

A clear path to substantial improvements in the separation performance of MOF-based MMMs can be related to increasing MOF loadings to an extent where diffusion pathways through an entire membrane become available only via MOF crystals and thin interfaces between the neighboring crystals. The availability of such pathways corresponds to the percolation over the MOF phase in MMMs, i.e., the existence of a spanning cluster of interconnected MOF crystals discussed above. In this work, we quantified for the first time the average sizes of clusters of interconnected MOF crystals and the intra-cluster diffusivity using microscopic diffusion measurements. It was observed that with increasing MOF loading there is a tendency for an increase of both the cluster sizes and intra-cluster diffusivity. The reported quantification of the MOF cluster growth as a function of MOF loading is required for a better understanding of the process of reaching conditions of percolation over the MOF phase in MMMs. Larger increases in the MOF loading leading to larger MOF clusters can require functionalization of the external MOF crystal surface to avoid occurrence of intra-membrane defects and to form mechanically stable MMMs. This approach will be explored in our future research.

4. Conclusion

^{13}C PFG NMR was applied to study the self-diffusion of CO_2 and CH_4 in UiO-66-NH_2/6FDA-Durene mixed matrix membranes as a function of increasing MOF loading. The PFG NMR measurements were performed for a broad range of diffusion times and the corresponding RMSDs, which were comparable to or larger than the average UiO-66-NH_2 crystal size. These diffusion studies demonstrated that as the MOF loading in the MMM is increased beyond 12.5 wt% of MOF, two molecular ensembles with different diffusivities and fractions are observed for both gases considered in this study: i) an ensemble corresponding to diffusion inside clusters of MOF crystals, and ii) an ensemble corresponding to diffusion mostly inside the polymer phase of the membrane samples. Quantification of the MOF cluster sizes revealed a direct correlation with the intra-membrane MOF loading. As the MOF loading increased, so did the cluster sizes. Furthermore, gas self-diffusivity inside clusters of MOF crystals showed a tendency to become larger with increasing MOF loading. The latter increase can be related to a tighter packing of MOF crystals inside the clusters and creation of some free volume defects at the interfaces between the neighboring MOF crystals with an increase in the MOF loading. Functionalization of the external surface of MOF crystals to improve the properties of the interfaces in such clusters will be explored in our future research.

CRediT authorship contribution statement

Omar Boloki: Writing – review & editing, Writing – original draft, Investigation, Formal analysis, Data curation. **Stephen Dewitt:** Writing – review & editing, Investigation, Formal analysis, Data curation. **Eric T. Hahnert:** Writing – review & editing, Investigation, Formal analysis, Data curation. **Zachary Smith:** Writing – review & editing, Supervision, Methodology, Investigation, Funding acquisition, Conceptualization. **Sergey Vasenkov:** Writing – review & editing, Writing – original draft, Supervision, Methodology, Investigation, Funding acquisition, Formal analysis, Conceptualization.

Declaration of competing interest

All authors of this manuscript certify that they have NO affiliations with or involvement in any organization or entity with any financial interest (such as honoraria; educational grants; participation in speakers' bureaus; membership, employment, consultancies, stock ownership, or other equity interest; and expert testimony or patent-licensing arrangements), or non-financial interest (such as personal or professional relationships, affiliations, knowledge or beliefs) in the subject matter or materials discussed in this manuscript.

Data availability

Data will be made available on request.

Acknowledgements

The present work was financially supported by NSF (CBET award No. 2034734 and 2034742). A portion of this work was performed in the McKnight Brain Institute at the National High Magnetic Field Laboratory's Advanced Magnetic Resonance Imaging and Spectroscopy (AMRIS) Facility, which is supported by National Science Foundation Cooperative Agreement DMR-1644779, DMR-2128556 and the State of Florida. This work was supported in part by an NIH award, S10 RR031637, for magnetic resonance instrumentation.

Appendix A. Supplementary data

Supplementary data to this article can be found online at https://doi.org/10.1016/j.micromeso.2024.113249.

References

[1] D.S. Sholl, R.P. Lively, Seven chemical separations to change the world, Nature 532 (2016) 435–437, https://doi.org/10.1038/532435a.

[2] R.W. Baker, K. Lokhandwala, Natural gas processing with membranes: an overview, Ind. Eng. Chem. Res. 47 (2008) 2109–2121, https://doi.org/10.1021/ie071083w.

[3] M. Galizia, W.S. Chi, Z.P. Smith, T.C. Merkel, R.W. Baker, B.D. Freeman, 50th anniversary perspective: polymers and mixed matrix membranes for gas and vapor separation: a review and prospective opportunities, Macromolecules 50 (2017) 7809–7843, https://doi.org/10.1021/acs.macromol.7b01718.

[4] Q. Qian, P.A. Asinger, M.J. Lee, G. Han, K. Mizrahi Rodriguez, S. Lin, F. M. Benedetti, A.X. Wu, W.S. Chi, Z.P. Smith, MOF-based membranes for gas separations, Chem. Rev. 120 (2020) 8161–8266, https://doi.org/10.1021/acs.chemrev.0c00119.

[5] Y. Jiang, C. Liu, J. Caro, A. Huang, A new UiO-66-NH2 based mixed-matrix membranes with high CO2/CH4 separation performance, Microporous Mesoporous Mater. 274 (2019) 203–211, https://doi.org/10.1016/j.micromeso.2018.08.003.

[6] L.M. Robeson, Correlation of separation factor versus permeability for polymeric membranes, J. Membr. Sci. 62 (1991) 165–185, https://doi.org/10.1016/0376-7388(91)80060-J.

[7] L.M. Robeson, The upper bound revisited, J. Membr. Sci. 320 (2008) 390–400, https://doi.org/10.1016/j.memsci.2008.04.030.

[8] K. Chen, K. Xu, L. Xiang, X. Dong, Y. Han, C. Wang, L.-B. Sun, Y. Pan, Enhanced CO2/CH4 separation performance of mixed-matrix membranes through dispersion of sorption-selective MOF nanocrystals, J. Membr. Sci. 563 (2018) 360–370, https://doi.org/10.1016/j.memsci.2018.06.007.

[9] Q. Qian, A.X. Wu, W.S. Chi, P.A. Asinger, S. Lin, A. Hypsher, Z.P. Smith, Mixed-matrix membranes formed from imide-functionalized UiO-66-NH2 for improved interfacial compatibility, ACS Appl. Mater. Interfaces 11 (2019) 31257–31269, https://doi.org/10.1021/acsami.9b07500.

[10] R. Mueller, V. Hariharan, C. Zhang, R. Lively, S. Vasenkov, Relationship between mixed and pure gas self-diffusion for ethane and ethene in ZIF-8/6FDA-DAM mixed-matrix membrane by pulsed field gradient NMR, J. Membr. Sci. 499 (2016) 12–19, https://doi.org/10.1016/j.memsci.2015.10.036.

[11] H. Daglar, S. Aydin, S. Keskin, MOF-based MMMs breaking the upper bounds of polymers for a large variety of gas separations, Separ. Purif. Technol. 281 (2022) 119811, https://doi.org/10.1016/j.seppur.2021.119811.

[12] E.M. Forman, A. Baniani, L. Fan, K.J. Ziegler, E. Zhou, F. Zhang, R.P. Lively, S. Vasenkov, Ethylene diffusion in crystals of zeolitic imidazole Framework-11 embedded in polymers to form mixed-matrix membranes, Microporous Mesoporous Mater. 274 (2019) 163–170, https://doi.org/10.1016/j.micromeso.2018.07.044.

[13] V. Muthukumaraswamy Rangaraj, M.A. Wahab, K.S.K. Reddy, G. Kakosimos, O. Abdalla, E.P. Favvas, D. Reinalda, F. Geuzebroek, A. Abdala, G.N. Karanikolos, Metal organic framework — based mixed matrix membranes for carbon dioxide separation: recent advances and future directions, Front. Chem. 8 (2020), https://doi.org/10.3389/fchem.2020.00534.

[14] W. Chai, Y. Shen, J. Wang, G. Zhang, Applications of metal-organic framework materials, J. Phys. Conf. Ser. 2194 (2022) 012014, https://doi.org/10.1088/1742-6596/2194/1/012014.

[15] J. Winarta, B. Shan, S.M. McIntyre, L. Ye, C. Wang, J. Liu, B. Mu, A decade of UiO-66 research: a historic review of dynamic structure, synthesis mechanisms, and characterization techniques of an archetypal metal–organic framework, Cryst. Growth Des. 20 (2020) 1347–1362, https://doi.org/10.1021/acs.cgd.9b00955.

[16] J.H. Cavka, S. Jakobsen, U. Olsbye, N. Guillou, C. Lamberti, S. Bordiga, K. P. Lillerud, A new zirconium inorganic building brick forming metal organic frameworks with exceptional stability, J. Am. Chem. Soc. 130 (2008) 13850–13851, https://doi.org/10.1021/ja8057953.

[17] M. Kandiah, M.H. Nilsen, S. Usseglio, S. Jakobsen, U. Olsbye, M. Tilset, C. Larabi, E.A. Quadrelli, F. Bonino, K.P. Lillerud, Synthesis and stability of tagged UiO-66 Zr-MOFs, Chem. Mater. 22 (2010) 6632–6640, https://doi.org/10.1021/cm102601v.

[18] M.Z. Ahmad, M. Navarro, M. Lhotka, B. Zornoza, C. Téllez, W.M. de Vos, N. E. Benes, N.M. Konnertz, T. Visser, R. Semino, G. Maurin, V. Fila, J. Coronas, Enhanced gas separation performance of 6FDA-DAM based mixed matrix membranes by incorporating MOF UiO-66 and its derivatives, J. Membr. Sci. 558 (2018) 64–77, https://doi.org/10.1016/j.memsci.2018.04.040.

[19] G.E. Cmarik, M. Kim, S.M. Cohen, K.S. Walton, Tuning the adsorption properties of UiO-66 via ligand functionalization, Langmuir 28 (2012) 15606–15613, https://doi.org/10.1021/la3035352.

[20] J. Winarta, A. Meshram, F. Zhu, R. Li, H. Jafar, K. Parmar, J. Liu, B. Mu, Metal–organic framework-based mixed-matrix membranes for gas separation: an overview, J. Polym. Sci. 58 (2020) 2518–2546, https://doi.org/10.1002/pol.20200122.

[21] R. Mueller, S. Zhang, C. Zhang, R. Lively, S. Vasenkov, Relationship between long-range diffusion and diffusion in the ZIF-8 and polymer phases of a mixed-matrix membrane by high field NMR diffusometry, J. Membr. Sci. 477 (2015) 123–130, https://doi.org/10.1016/j.memsci.2014.12.015.

[22] V. Nafisi, M.-B. Hägg, Gas separation properties of ZIF-8/6FDA-durene diamine mixed matrix membrane, Separ. Purif. Technol. 128 (2014) 31–38, https://doi.org/10.1016/j.seppur.2014.03.006.

[23] M. Dvoyashkin, J. Zang, G.I. Yucelen, A. Katihar, S. Nair, D.S. Sholl, C.R. Bowers, S. Vasenkov, Diffusion of tetrafluoromethane in single-walled aluminosilicate nanotubes: pulsed field gradient NMR and molecular dynamics simulations, J. Phys. Chem. C 116 (2012) 21350–21355, https://doi.org/10.1021/jp3054247.

[24] E.M. Forman, B.R. Pimentel, K.J. Ziegler, R.P. Lively, S. Vasenkov, Microscopic diffusion of pure and mixed methane and carbon dioxide in ZIF-11 by high field diffusion NMR, Microporous Mesoporous Mater. 248 (2017) 158–163, https://doi.org/10.1016/j.micromeso.2017.04.041.

[25] A. Baniani, M.P. Rivera, J. Marreiros, R.P. Lively, S. Vasenkov, Influence of polymer modification on intra-MOF self-diffusion in MOF-based mixed matrix membranes, Microporous Mesoporous Mater. 359 (2023) 112648, https://doi.org/10.1016/j.micromeso.2023.112648.

[26] A. Baniani, M.P. Rivera, R.P. Lively, S. Vasenkov, Quantifying diffusion of organic liquids in a MOF component of MOF/Polymer mixed-matrix membranes by high field NMR, J. Membr. Sci. 640 (2021) 119786, https://doi.org/10.1016/j.memsci.2021.119786.

[27] R.M. Cotts, M.J.R. Hoch, T. Sun, J.T. Markert, Pulsed field gradient stimulated echo methods for improved NMR diffusion measurements in heterogeneous systems, J. Magn. Reson. 83 (1989) 252–266, https://doi.org/10.1016/0022-2364(89)90189-3.

[28] S.J. Gibbs, C.S. Johnson, A PFG NMR experiment for accurate diffusion and flow studies in the presence of eddy currents, J. Magn. Reson. 93 (1991) 395–402, https://doi.org/10.1016/0022-2364(91)90014-K.

[29] J. Kärger, D.M. Ruthven, D.N. Theodorou, Diffusion in Nanoporous Materials, Wiley-VCH, Weinheim, 2012.

[30] A. Baniani, S.J. Berens, M.P. Rivera, R.P. Lively, S. Vasenkov, Potentials and challenges of high-field PFG NMR diffusion studies with sorbates in nanoporous media, Adsorption 27 (2021) 485–501, https://doi.org/10.1007/s10450-020-00255-y.

[31] P. Duan, J.C. Moreton, S.R. Tavares, R. Semino, G. Maurin, S.M. Cohen, K. Schmidt-Rohr, Polymer infiltration into metal–organic frameworks in mixed-matrix membranes detected in situ by NMR, J. Am. Chem. Soc. 141 (2019) 7589–7595, https://doi.org/10.1021/jacs.9b02789.

[32] Q. Yang, H. Jobic, F. Salles, D. Kolokolov, V. Guillerm, C. Serre, G. Maurin, Probing the dynamics of CO2 and CH4 within the porous zirconium terephthalate UiO-66 (Zr): a synergic combination of neutron scattering measurements and molecular simulations, Chem. Eur J. 17 (2011) 8882–8889, https://doi.org/10.1002/chem.201003596.

[33] Y. Liu, G. Liu, C. Zhang, W. Qiu, S. Yi, V. Chernikova, Z. Chen, Y. Belmabkhout, O. Shekhah, M. Eddaoudi, W. Koros, Enhanced CO2/CH4 separation performance of a mixed matrix membrane based on tailored MOF-polymer formulations, Adv. Sci. 5 (2018) 1800982, https://doi.org/10.1002/advs.201800982.

[34] F. Aghili, A.A. Ghoreyshi, A. Rahimpour, B. Van der Bruggen, New chemistry for mixed matrix membranes: growth of continuous multilayer UiO-66-NH2 on UiO-66-NH2-based polyacrylonitrile for highly efficient separations, Ind. Eng. Chem. Res. 59 (2020) 7825–7838, https://doi.org/10.1021/acs.iecr.9b07063.

[35] C. Li, A. Qi, Y. Ling, Y. Tao, Y.-B. Zhang, T. Li, Establishing gas transport highways in MOF-based mixed matrix membranes, Sci. Adv. 9 (2023) eadf5087, https://doi.org/10.1126/sciadv.adf5087.

[36] Q. Qian, P.A. Asinger, M.J. Lee, G. Han, K. Mizrahi Rodriguez, S. Lin, F. M. Benedetti, A.X. Wu, W.S. Chi, Z.P. Smith, MOF-based membranes for gas separations, Chem. Rev. 120 (2020) 8161–8266, https://doi.org/10.1021/acs.chemrev.0c00119.

[37] C. Zhang, R.P. Lively, K. Zhang, J.R. Johnson, O. Karvan, W.J. Koros, Unexpected molecular sieving properties of zeolitic imidazolate framework-8, J. Phys. Chem. Lett. 3 (2012) 2130–2134, https://doi.org/10.1021/jz300855a.